Structural selection of ionic-complementary peptides with electrostatic interactions

Zhiqiang Yan, Jun Wang,[*,†] Jian Zhang, Meng Qin, and Wei Wang[*,‡]
National Laboratory of Solid State Microstructure and Department of Physics, Nanjing University, Nanjing 210093, China
(Received 24 February 2010; revised manuscript received 21 June 2010; published 30 September 2010)

The structures of the peptides and their assembly are largely modulated by the environment. To discover the physical principles governing the structural modulations of peptides by the environment would be useful for many applications. As the typical examples, the structures of three kinds of ionic-complementary EAK16-family peptides under various environmental conditions are studied with simulations in this work. A model with intermediate resolution is used, in which both the backbone hydrogen bonds and electrostatic interactions are explicitly considered. The thermodynamics of these peptides (including the free energy and heat capacity) are described for various strengths of the electrostatic interactions which reflect the variation of environment. With these results, the phase diagrams of these peptides related to the temperature and the strength of electrostatic interactions are presented and compared. Based on the differences in the phase structures of the peptide, the different aggregation behaviors are explained based on the monomeric structural features of the peptides. Through the analysis on the stability of various secondary structures of these peptides, it is demonstrated that the charge pattern is the basic reason of the different responses of the EAK16-family peptides to the environmental changes. These results provide some examples and insights for the principles of structural selection by environment and may be helpful for further analysis and designs of peptide systems.

DOI: 10.1103/PhysRevE.82.031917 PACS number(s): 87.14.ef, 87.15.ap, 87.15.bg

I. INTRODUCTION

Peptides are a kind of important molecules with many interests in biological, medical, and material fields [1–8]. Due to the simplicity of peptides in their sequences and interactions as well as in their manipulations, the peptides are often used to build various kinds of nanostructures with biological or technical applications [4–8]. These processes are widely modulated by the environmental factors, such as *p*H condition, salt concentrations, even neighboring peptides, and so on [8–24]. To discover the methods to adjust and control the structures of short peptides and to understand the underlying physics would be greatly valuable for developing more functional nanostructures with peptides [8,21–28].

One of the typical examples of peptide systems is the ionic-complementary peptides (such as the EAK16-family peptides as shown in Table I) which have been systematically studied during recent decades [12–21]. These designed peptides are built with order arrangements of charged amino acids. With various kinds of solution conditions (*p*H values or salt concentrations), the ionic-complementary peptides could form different kinds of aggregates due to the modulation of electrostatic interactions between side chains [13–17]. For example, the peptide EAK16-IV (the sequence as in Table I) could form globular aggregates at neutral *p*H levels between 6.5 and 7.5, but when the solution *p*H is lower than 6.5 or is higher than 7.5, the aggregates would take a fibrillar form [13]. These different aggregates originate from the variation of monomeric peptide structures in different environmental conditions [21]. More interestingly, with the same composition as the peptide EAK16-IV, the peptide EAK16-II (the sequence in Table I) has different behaviors under various *p*H conditions. It only forms fibrillar structures throughout the *p*H range from 4 to 11 [15,17]. These peptides have different responses to the environment variations. How does the environment modulate the structural formation of these peptides differently to produce various aggregates? What are the key factors which determine the ability to respond to the environmental variations? The answers to these questions would be valuable to understand the behavior of the EAK16-family peptides and may be helpful to provide some physical insights into the general principle of structural selection in peptide systems. Considering the experimental difficulties to solve these problems [29], a simulation study on EAK16-family peptides is carried out in this work as the approach for these problems.

In this work, dynamic simulations are carried out for three kinds of simplified ionic EAK16-family peptides with a protein model with an intermediate resolution. It is found that these peptides may adopt various kinds of secondary structures at different temperatures and with different strengths of electrostatic interactions which mimic the solution condition. The differences between various peptides are discussed based on kinetics and the free-energy landscapes of these peptides. Based on the thermodynamic information, the phase diagrams of these peptides related to the temperature and the strength of electrostatic interaction are given out. These phase diagrams are compared in detail. These results

TABLE I. Sequences of the ionic-complementary EAK16-family peptides.

Name	Sequence
EAK16-I	AEAKAEAKAEAKAEAK
EAK16-II	AEAEAKAKAEAEAKAK
EAK16-IV	AEAEAEAEAKAKAKAK

*Corresponding author.
†wangj@nju.edu.cn
‡wangwei@nju.edu.cn

outline a physical picture of how the environmental factor modulates the conformational responses of the EAK16-family peptides. Besides, the relative stability of the EAK16-family peptides to adopt certain secondary structures is discussed. The information about the structural preferences of these EAK-family peptides qualitatively explains the aggregation features of these peptides. These results demonstrate the important contribution of the sequential pattern in structural selection. All these features for the EAK16-family peptides provide some useful insights into the underlying physics governing the selections and modulations of secondary structures in proteins.

II. MODELS AND METHODS

A. Model for the EAK16-family peptides

EAK16-family peptides are all composed of the amino acids of the glutamic acid (E), the alanine (A), and the lysine (K). The side chains of the amino acids E and K are all charged in the neutral solution condition. The electrostatic interaction takes an important role for these peptide systems. At the same time, the backbone hydrogen bond is another important ingredient to affect the secondary structures. These two kinds of interactions act as the necessary parts to describe the EAK16-family peptide systems. In this work, a minimal model with explicit descriptions for the above interactions is used. This model captures the main physics of the EAK16-family peptides and reduces the computational demands.

In this model, all the heavy (nonhydrogen) atoms are explicitly represented except that the side chain of each residue is described by a single bead for simplicity, as shown in Fig. 1(a). Different from the regular off-lattice models, the explicit inclusion of side chains may introduce proper chirality for amino acids as well as a more precise center for side-chain-related interactions [30–32]. It is worth pointing out that the polar hydrogen connected to nitrogen (N) can be calculated uniquely based on the rigid geometry of peptide plane. Therefore, this kind of model empowers an explicit representation for hydrogen bonds with the atoms C, N, and O in the peptide-bond plane. Based on the five-bead representation of residues, the Hamiltonian for the peptide systems has four parts of contributions, including the covalent binding between atoms H_{covalent}, the hydrogen bonds $H_{\text{H bond}}$, the electrostatic interactions H_{elec}, and the hard-core repulsion of atoms H_{core}, that is,

$$H = H_{\text{covalent}} + H_{\text{H bond}} + H_{\text{elec}} + H_{\text{core}}. \tag{1}$$

As a remark, the hydrophobic effect is not considered in present model since there are no large hydrophobic amino acids in the composition of peptides.

For the covalent interactions, a series of bonds and pseudobonds are constructed to mimic the chemical bonds and angular dependence of peptide chains. These bonds are realized with infinitely high potential wells,

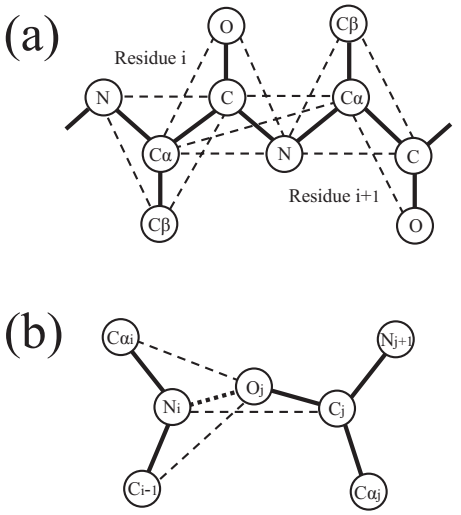

FIG. 1. (a) Schematic diagram of the five-bead model. The thick solid lines represent the covalent and the peptide bonds. The dashed lines represent the pseudobonds which are used to maintain backbone bond angles, consecutive C_α distances, and residue L isomerization. (b) Schematic diagram of the hydrogen bond among backbone. The thick dashed line is the hydrogen bond. The thin dashed lines are the pseudocontacts which are introduced to mimic the collinear structure of group *CO* and *NH* in real proteins.

$$H_{\text{covalent}}(r_{\mu\nu}) = \begin{cases} 0, & 1-\delta < \dfrac{r_{\mu\nu}}{d_{s_\mu s_\nu}} \le 1+\delta \\ \infty, & \text{otherwise}, \end{cases} \tag{2}$$

where s_μ represents the type of the bead μ, $r_{\mu\nu}$ is the distance between beads μ and ν, d_{pq} is the bond length between the beads of types p and q, and δ is the tolerance of bond or pseudobond length which is regularly set as 0.02. The parameters $\{d_{pq}\}$ are chosen based on the data from protein structures. The details of these parameters are given in the literature [21]. Similar parameters have been used in other studies [32].

Different from the bond or pseudobond interactions, the hydrogen bond behaves more complicatedly. The concerned atoms C, O, and N and the related polar hydrogen prefer to have a collinear configuration due to the nature of the hydrogen bond. Here, a realization same as that in Ref. [33] is adopted. In detail, four pseudocontacts N^i-O^j, N^i-C^j, C^{i-1}-O^j, and C^i_α-O^j, are defined, as shown in Fig. 1(b). Each pseudocontact T is established when the distance D_T of two concerned atoms is within the corresponding range $[D_T^{\min}, D_T^{\max}]$. A corresponding energetic factor is defined as

$$E_T = \begin{cases} 0, & D_T > D_T^{\max} \\ -1, & D_T^{\min} \le D_T \le D_T^{\max} \\ \infty, & D_T < D_T^{\min}. \end{cases} \tag{3}$$

The hydrogen bond would come into being only when all the four pseudocontacts are formed. The corresponding energy could be defined as

TABLE II. The parameters for the pseudocontacts related to the hydrogen bonds.

Pseudocontact	N^i-O^j	N^i-C^j	C^{i-1}-O^j	C^i_α-O^j
$D^{\min}$ (Å)	2.80	3.80	3.60	3.60
$D^{\max}$ (Å)	3.12	4.23	4.00	4.04

$$H_{\text{H bond}} = -\epsilon_{\text{HB}} \left| \prod_T E_T \right|, \tag{4}$$

in which T runs over four pseudocontacts mentioned above and ϵ_{HB} is the strength of hydrogen bonds. This strength ϵ_{HB} is taken as the energetic unit in our work. The detailed parameters for the pseudocontacts are given in Table II, which has been used in the literature [21].

Electrostatic interaction is another important nonbonded interaction in this system. In this model, the charge is placed at the center of the bead which mimics the side chain. Only the charges of glutamic acids and lysines are considered in the model. Considering the screening effect of solvent waters, a distance-dependent dielectric constant is employed as $\varepsilon_{dielec} \propto r$, where r is the distance between the concerned charges. Therefore, the electrostatic interaction would have the form of r^{-2} [34]. Since this kind of interaction decays rather slow, a multiple-step function is used,

$$H_{\text{elec}}(r) = \begin{cases} 0, & r > d_M \\ u_k \epsilon_{\text{elec}}, & d_k \le r \le d_{k+1} \quad (k = 1, \ldots, M-1) \\ \infty, & r < d_1, \end{cases} \tag{5}$$

in which ϵ_{elec} is the strength of electrostatic interaction, the distance set $\{d_k : k=1, \ldots, M\}$ describes the location of steps, and u_k $(k=1, \ldots, M-1)$ is the corresponding energetic parameter. In our model, $M=6$ steps are chosen, and the corresponding parameters $\{d_k\}$ and $\{u_k\}$ are given in Table III, which are determined by fitting the function r^{-2}. This kind of interaction is also used in the simulations for EAK16-family peptides [21]. Here, it is worth noting that the strength $|\epsilon_{\text{elec}}| = \chi$ reflects the charge condition of the concerned amino acids. In the acidic or basic solutions, some amino acids may be protonized or deprotonated, which may reduce the concerned charges. This would produce a smaller strength $|\epsilon_{\text{elec}}|$. Meanwhile, the neutral condition would correspond to the case with large $|\epsilon_{\text{elec}}|$. The similar considerations have been applied in some other modeling for the effect of denaturants [35]. In this sense, the parameter $|\epsilon_{\text{elec}}|$ is used as a reflection of the environment condition in our model. Based on the estimated values of hydrogen bonding energy and electrostatic interaction [36–39], the strength $\chi = 0.5$ is taken to mimic the neutral condition, and the strength between 0 and 0.5 corresponds to the condition in acidic or basic solution.

TABLE III. The parameters for the step function related to the electrostatic interactions.

k	1	2	3	4	5	6
d_k (Å)	4.4	4.8	5.7	6.8	9.2	15.0
$u_k(\epsilon_{\text{HB}})$	1.00	0.77	0.54	0.33	0.14	

Besides the above interactions which concern some specific atoms, the hard-core interaction is unique for all pairs of atoms to realize the exclusive-volume effect. The hard-core interaction between the atoms μ and ν generally has the form

$$H_{\text{core}}(r_{\mu\nu}) = \begin{cases} 0, & r_{\mu\nu} > R_{\text{core}} \\ \infty, & \text{otherwise}, \end{cases} \tag{6}$$

where R_{core} shows the size of repulsive core and is regularly determined as the summation of the radii of the concerned atoms, $R_{\text{core}} = R_\mu + R_\nu$. The radii of various atoms could be referred to the literature [21].

As a comparison, an uncharged model of EAK16-family peptide (uEAK16) is also used, in which electrostatic interaction is omitted. This model mimics the extreme condition with $\chi = 0$. All the other interactions are the same as the above model for EAK16-family peptides. The comparisons between EAK16 and uEAK16 models provide a way to study the effect of electrostatic interactions on the formation of secondary structures.

B. Discrete molecular dynamics

To be compatible with our discontinuous potentials, the event-driven discrete molecular dynamics (DMD) [40–43] are used in our simulations. The collisions and propagations of the beads are proceeded sequentially, and all these events build up the kinetics of systems. The discontinuous feature of potentials makes the propagation be the motion with constant speed, and thus, in the processing of the events all are algebra calculations rather than the integration of dynamic equations, which greatly reduces the computational demands. It is worth noting that the event-driving feature makes the time of evolution not a counting of the number of the collisions but a summation of times of all propagations. The time unit is defined as $\tau_0 = \sigma_0 \sqrt{m_0 / \epsilon_{\text{HB}}}$, where σ_0 is the unit length (=1 Å). In our DMD simulations, constant-temperature ensemble is realized with Andersen's method [31,44,45]. The number of the collisions with ghost particles is controlled as about 1% of all collisions, which ensures the thermodynamic equilibrium.

C. Weighted histogram analysis method

Weighted histogram analysis method (WHAM) is employed to calculate the thermodynamic properties [45,46]. In this method, a series of histograms obtained from thermodynamic sampling could be utilized together to find out the density of states and the partition functions based on a self-consistent method. With this kind of method, the statistical errors could be minimized, which greatly extends the validity of results for a large range of temperatures. For our discontinuous potential, we generally take the minimal interval (often 0.1) of energy spectrum as the bin size of the histograms.

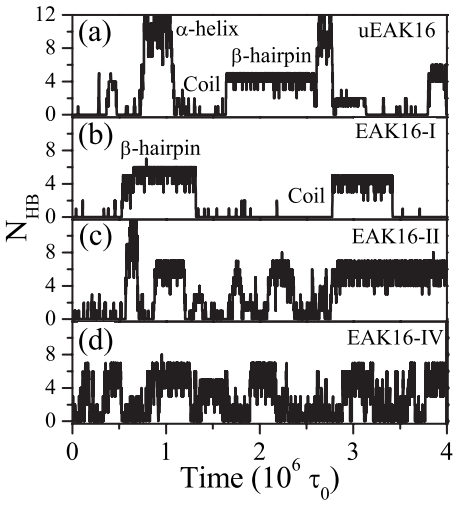

FIG. 2. Kinetic trajectories of various EAK16-family peptides (a) for uEAK1616 at $T=0.128$, (b) for EAK16-I at $T=0.135$, (c) for EAK16-II at $T=0.141$, and (d) for EAK16-IV at $T=0.167$. For the cases of (b)–(d), $\chi=0.5$. The helix, hairpin, and coil states are marked along the trajectories.

III. RESULTS AND DISCUSSIONS

A. Folding kinetics and thermodynamics of EAK16-family peptides

By varying the strength of electrostatic interactions, the modulation of solution *p*H condition could be simulated. In this work, a series of DMD simulations are carried out for various χ (from 0 to 0.5). For each parameter χ, several trajectories at various temperatures from 0.1 to 0.2 are implemented for WHAM analysis. To avoid the bias of the initial conformations, all the simulations are started from the random conformations obtained from high-temperature simulations (regularly $T \geq 0.5$).

Some typical trajectories for various EAK16-family peptides (including uEAK16 model) are given in Fig. 2. For EAK16-I, EAK16-II, and EAK16-IV, a large strength $\chi=0.5$ is used to mimic the neutral solution condition. For each trajectory, the running temperature (as in the caption of Fig. 2) is selected so that the random-coil conformations (extended with few random hydrogen bonds, noted as $\mathcal{C}$ type) take up almost half of the simulation times. These kinds of temperatures are similar as the melting temperature of regular proteins. At these temperatures, a large part of conformational space could be explored during simulations. From these trajectories, it is observed that there are two other kinds of populations besides the $\mathcal{C}$-type state based on the number of hydrogen bonds N_{HB}, one around $N_{\mathrm{HB}}=12$ and the other around $N_{\mathrm{HB}}=6$. By analyzing the conformations in trajectories, it is found that these two populations have different patterns of hydrogen bonds. In detail, the conformations with their N_{HB} around 12 have rich α-helical content. The hydrogen bonds are generally between the i and $(i+4)$th residues. This kind of states are noted as $\mathcal{H}$-type state. Meanwhile, the conformations with $N_{\mathrm{HB}}=6$ have many ladderlike patterns of hydrogen bonds, including the β-hairpin structures. These states are noted as $\mathcal{P}$-type state. Clearly, not all these states could be observed in all EAK16-family peptides. The uEAK16 model has clear distributions of these three kinds of states. Differently, the distributions of the other EAK16-family peptides are biased. For the EAK16-II peptide, the $\mathcal{H}$-type state still can be observed, but the population is suppressed. While for EAK16-I and EAK16-IV peptides, there are not $\mathcal{H}$-type states in the whole simulations. These demonstrate that the electrostatic interaction would bias toward the β-hairpin-like conformations. The differences between EAK16-II and EAK16-I, IV also suggest that the electrostatic interactions have weaker effect on the EAK16-II peptides. This supports the experiments that various sequential patterns may have different responses to environment changes and that the environment has weaker modulation for EAK16-II peptides [15].

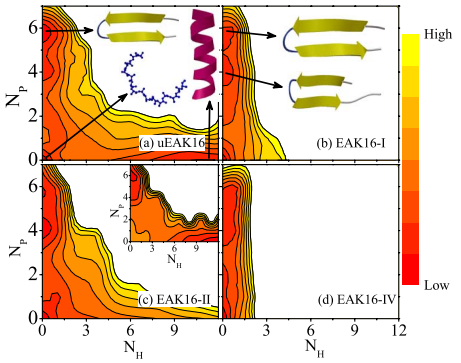

FIG. 3. (Color online) Free energy landscapes in terms of $N_{\mathcal{H}}$ and $N_{\mathcal{P}}$ at melting temperatures. The peptides and the corresponding parameters for (a)–(d) are the same as those for Fig. 2. A landscape of EAK16-II at relatively low temperature ($T=0.124$) is given in the inset of (c). Some typical conformations are marked.

This kind of conformational distributions could also be visualized more quantitatively from the free-energy landscapes spanned with the numbers of various kinds of hydrogen bonds, $N_{\mathcal{H}}$ and $N_{\mathcal{P}}$ (as shown in Fig. 3). Here, $N_{\mathcal{H}}$ ($N_{\mathcal{P}}$) is the number of hydrogen bonds which exist in $\mathcal{H}$- ($\mathcal{P}$-) type states. The temperatures and interaction parameters are the same as those for Fig. 2. Consistent with kinetic trajectories, uEAK16 peptide has three minima corresponding to $\mathcal{C}$, $\mathcal{H}$, and $\mathcal{P}$ states, as shown in Fig. 3(a). The typical conformations are presented. The depths for $\mathcal{H}$- and $\mathcal{P}$-type states are similar. This implies that there are no preferences to certain secondary structures without electrostatic interactions at that temperature. While including the electrostatic interactions, the landscapes would vary depending on the sequences. The landscape of EAK16-II peptide is the most similar one to that of uEAK16 model, as shown in Fig. 3(c), except that the minimum for $\mathcal{H}$-type states becomes rather shallow. The existence of the minimum related to $\mathcal{H}$-type states could be further approved on the landscape at a lower temperature $T=0.124$ [as the inset of Fig. 3(c)]. At the low temperature, the helical states are clearly stabilized. Differently, this minimum for $\mathcal{H}$-type states disappears for EAK16-I or EAK16-IV, as in Figs. 3(b) and 3(d), and this kind of phenomenon would still be kept for higher or lower temperatures (data are not shown). These also demonstrate the bias due to the electrostatic interaction and are consistent with the observations from the kinetic trajectories.

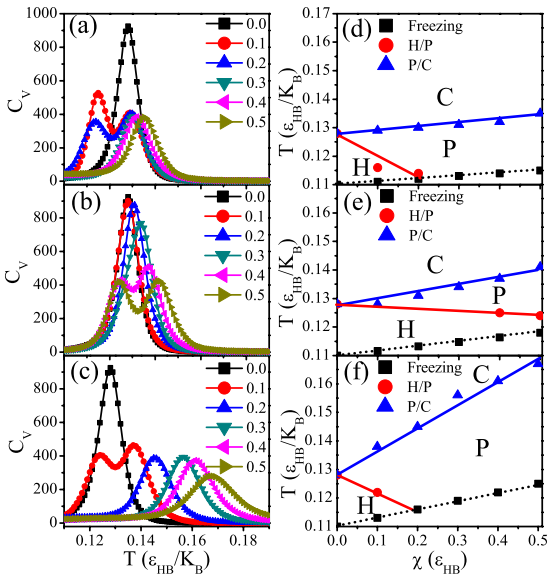

FIG. 4. (Color online) The heat capacities and phase diagrams for EAK16-family peptides. The heat capacities with various χ (from 0 to 0.5) are given (a) for EAK16-I, (b) for EAK16-II, and (c) for EAK16-IV at various temperatures (as marked with different symbols). The phase diagrams are also derived (d) for EAK16-I, (e) for EAK16-II, and (f) for EAK16-IV. The phase boundaries are marked with different symbols. The most stable states ($\mathcal{C}$, $\mathcal{H}$, or $\mathcal{P}$) are marked in the corresponding diagrams. In the phase diagrams, the freezing are represented with the dashed lines.

B. Phase diagrams of EAK16-family peptides

Besides the comparisons between the peptides at their melting temperatures, it would be more informative to investigate the thermodynamic behaviors of these peptides in a wide range of temperatures. The temperature-dependent heat capacities of the peptides are calculated with WHAM method for various strengths χ of electrostatic interactions, as shown in Figs. 4(a)–4(c). Considering the competitions between various kinds of secondary structures, the peaks indicate the transitions between various secondary structures. These transitions are marked and connected on the T-χ plane. This gives out the phase diagrams for these EAK16-family peptides, as shown in Figs. 4(d)–4(f). On these phase diagrams, each isolated region is marked with the symbol representing the stablest secondary structure. For each peptide, when the simulation temperature is lower than a certain temperature, the peptide would freeze in a certain secondary structure with little fluctuation in a long simulation ($4 \times 10^6 \tau_0$ which is approximately an order larger than the regular transition time between secondary structures). The frozen structures generally depend on the initial conformations. This freezing temperature is also marked in the phase diagram with dashed lines. Due to the same composition of these peptides, the lines related to freezing are almost the same for three kinds of peptides. It is worth noting that there are regularly metastable states for each phase. As illustrated in the landscapes in Fig. 2, there are multiple minima corresponding to various secondary structures. Therefore, the transitions across the boundary are generally of first order. These kinds of transitions are also observed in the similar systems [21,32]. With these phase diagrams, the whole thermodynamic information of these peptide systems is outlined.

For a small strength χ, three kinds of EAK16-family peptides have the similar behaviors of phase transitions, namely, the $\mathcal{C}/\mathcal{P}$ transition (at a relatively higher temperature) and $\mathcal{P}/\mathcal{H}$ transition (at a lower temperature). This may be attributed to the fact that helical structures have more hydrogen bonds compared with the hairpinlike structures. The differences of the stability of various secondary structures produce this kind of phase structure. Following the increase of the strength χ, the temperature for $\mathcal{C}/\mathcal{P}$ transition moves higher, while the temperature for $\mathcal{P}/\mathcal{H}$ transition decreases. This produces a wide region of $\mathcal{P}$ phase and a shrinking $\mathcal{H}$ phase. This is consistent with the observations on the kinetics and free-energy landscapes for these peptides. Yet, there are some differences between these peptides. First, the decrease rates of the temperatures for $\mathcal{P}/\mathcal{H}$ transition of EAK16-I and EAK16-IV are apparently larger than that of EAK16-II. Therefore, when χ is large than a certain value ($\sim$0.2), the phase boundary between $\mathcal{P}$ phase and $\mathcal{H}$ phase for EAK16-I and EAK16-IV would intersect with the line indicating freezing, and the $\mathcal{H}$ phase would diminish. As a result, for a large strength χ, there would be only one transition between $\mathcal{C}$ phase and $\mathcal{P}$ phase for EAK16-I and EAK16-IV. Second, the increase rates of the temperatures for $\mathcal{C}/\mathcal{P}$ transition of EAK16-I and EAK16-II are smaller than that of EAK16-IV. This indicates that the hairpin structure of EAK16-IV peptide is more preferred by the electrostatic interaction. At the same temperature, the EAK16-I and EAK16-II would have more chances to adopt the extended conformations. This is consistent with the previous analysis [15]. These thermodynamic characteristics outline the diverse responses to the variation of environment. These three EAK16-family peptides would vary their secondary structures from $\mathcal{P}$ state to $\mathcal{C}$ state (or $\mathcal{H}$ state) following the decrease of χ (namely, the variation of pH condition). The critical strengths related to the transition would vary largely for various peptides since the slopes of the phase boundary are rather different for these peptides. These phase diagrams provide a quantitative description for the responses of peptides to the environmental changes.

Based on these phase diagrams, the different aggregation properties of EAK16-family peptides could be explained. For the EAK16-IV peptide, the suppression of the coil and helical conformations makes the peptide probably take hairpin conformation with stronger electrostatic interaction. This kind of conformation would prevent the formation of large-scale fibrils and may induce the irregular aggregates. Therefore, EAK16-IV peptides may form globule aggregates at neutral solution conditions (corresponding to large χ). This is consistent with the experiment with FTIR spectrum, in which a signal of turn structure is observed [15]. While for EAK16-I and EAK16-II, the $\mathcal{C}/\mathcal{P}$ transitions all vary gently. They have larger preferences to coil structure at the room temperature compared with EAK16-IV. Therefore, only fibril structures are observed for various pH conditions [15–17]. Since the arrangement of charges in EAK16-I enables more turn structures, the EAK16-I peptide could form many hairpinlike structures with part of the chain. These structures could also hinder the formation of fibril structures. This kind

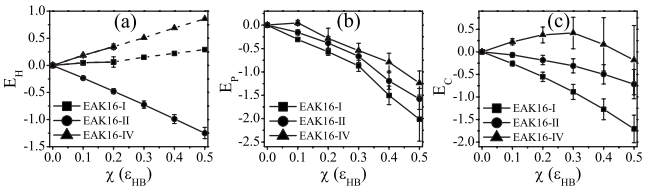

FIG. 5. Electrostatic energy, (a) $E_{\mathcal{H}}$, (b) $E_{\mathcal{P}}$, and (c) $E_{\mathcal{C}}$, for various kinds of states. The data for various peptides are represented with filled squares (EAK16-I), circles (EAK16-II), and triangles (EAK16-IV).

of situation would be relatively rare for EAK16-II and EAK16-IV. Therefore, EAK16-I has a larger critical aggregation concentration than that of EAK16-II, and the resultant fibrils are relatively rough [16,17]. The information from the phase diagrams and structures of peptides provides useful clues to understand the aggregation behaviors of EAK16-family peptides.

C. Selection for secondary structures by electrostatic interactions

How does the variation of electrostatic interaction realize the selection of the secondary structures? Based on the thermodynamic considerations, the competition of these secondary structures would be tightly related to the stability of various kinds of structures. To evaluate the contribution of the electrostatic interaction on the stability, the electrostatic energy $E_X^Y(\chi)$ of the peptide Y in the X-type states ($X=\mathcal{C}$, $\mathcal{P}$, or $\mathcal{H}$) is calculated by averaging over trajectories, as shown in Fig. 5. The simulation temperatures are picked up above the freezing temperature. The results are not sensitive to the selection of temperatures. Since the backbone interactions are similar for these peptides, E_X^Y describes the stability of the X-type conformations properly. For a transparent view, the representative conformations of the H-, P-, and C-type states obtained from the simulations are presented in Fig. 6. It is

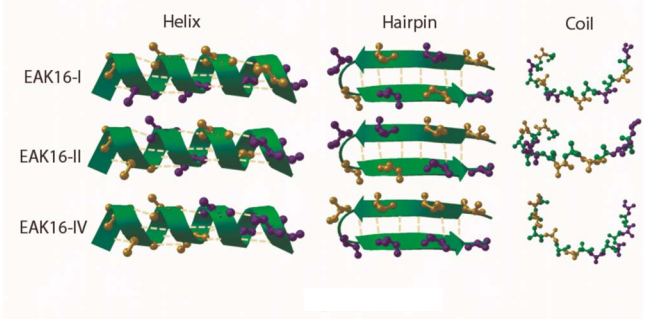

FIG. 6. (Color online) Typical conformations of $\mathcal{H}$-, $\mathcal{P}$-, and $\mathcal{C}$-type states for EAK16-family peptides. The charged residues are shaped with sticks and balls and colored based on their types: red for E and blue for K. The hydrogen bonds are marked as dashed lines. There are 12 hydrogen bonds between i and $(i+4)$th residues for the representative α-helix conformation of H type and 6 ladderlike hydrogen bonds for the representative β-hairpin conformation of P type, generally no hydrogen bonds for the random-coil conformations of C type.

TABLE IV. The average distances for the charged residues to its nearest attractive partners in typical $\mathcal{H}$- and $\mathcal{P}$-type structures.

Type	EAK16-I	EAK16-II	EAK16-IV
D_H (Å)	7.12	6.57	8.90
D_P (Å)	6.10	5.60	5.20

noted that there are no $\mathcal{H}$-type samples for peptides EAK16-I and EAK16-IV for large χ due to freezing. The corresponding data are calculated based on the conformations obtained with small χ and are marked with dashed lines in Fig. 5(a).

Based on the variation of the electrostatic interaction, it is found that the electrostatic interaction could stabilize the helical conformations of EAK16-II peptide but destabilize those of EAK16-I and EAK16-IV. This is related to the charge pattern in peptides as indicated on the representative helical conformations in Fig. 6. As well known, for the $\mathcal{H}$-type structures, the hydrogen bonds are formed between ith and $(i+4)$th residues. In EAK16-II peptide, the charges of residues related to the hydrogen bonds are also in different signs. The electrostatic would strengthen the hydrogen bonds and stabilize the helical structures. Differently, for the EAK16-I and EAK16-IV, the electrostatic interaction disfavors the hydrogen bonds in the $\mathcal{H}$-type structures, which produces a positive slope for $E_{\mathcal{H}}$. Therefore, when the electrostatic interaction is strong enough, the $\mathcal{H}$-type structures would be totally destabilized. These kinds of differences explain the elimination of $\mathcal{H}$-type phases at high-χ regions for EAK16-I and EAK16-IV. For the hairpinlike structures, the electrostatic interaction has the similar effects for these peptides due to their complementary feature of charges on the two arms of the hairpin. Since the distances between the charged side chains of the nearest attractively interacting residues in the hairpin conformations are shorter than those is helical conformations, as shown in Table IV, the increase of the electrostatic interaction is a little larger for $E_{\mathcal{P}}$ compared with $E_{\mathcal{H}}$, as shown in Figs. 5(a) and 5(b). This reflects that the hairpin conformations have more flexibility to fit their interactions and explains the enlargement of the $\mathcal{P}$ phases in the phase diagrams of various peptides. Meanwhile, for $\mathcal{C}$-type conformations, as shown in Fig. 5(c), the peptides show another kind of response to the variation of electrostatic interactions. The $E_{\mathcal{C}}$ for the peptides EAK16-I and EAK16-II decreases almost linearly, while the coil structures of EAK16-IV are destabilized. This is because that the long segments with same charges in EAK16-IV increase the stiffness of chains. The fluctuation in $\mathcal{C}$-type state would introduce some energetic penalties due to electrostatic repulsion. For large χ, the $\mathcal{C}$-type interaction between the residues with long sequential separation would compete with the local stiffness. This results in the decrease and large fluctuations of $E_{\mathcal{C}}$ in large-χ region. Since the amino acids E and K are arranged in an interlacing manner in EAK16-I and EAK16-II, these peptides behave normally. Based on this knowledge, it is easy to understand the differences of $\mathcal{C}/\mathcal{P}$ transitions in the phase diagrams. It is noticed that the electrostatic interaction would favor the peptide EAK16-II compared with EAK16-I. It suggests that the interactions in $\mathcal{C}$-type confor-

mations generally involve the residues with their sequential separations larger than 4, which would be favorite by EAK16-II. This is consistent with the experimental observations about the different critical aggregation concentrations of the peptides EAK16-I and EAK16-II [16,17]. This also provides us some insights about the features of backbone topology in coil-like conformations.

Through these comparisons, it is found that various peptides have different responses to the variation of electrostatic interactions. For EAK16-I, the helical structures are destabilized. For EAK16-IV, the hairpin structures are stabilized compared with other conformations. Moreover, for EAK16-II, there are no large variations in the relation between various secondary structures. The phase structures of these peptides thus vary accordingly, such as the $\mathcal{H}$ phase is suppressed for EAK16-I peptide, $\mathcal{P}$ phase is enlarged for EAK16-IV, and there are slight changes for the phase structure of EAK16-II. The stability variation depicts the competition between various secondary structures and outlines the basic reason for the structural selection.

More generally, all these kinds of variations are the results of the competitions between the nonspecific backbone interaction and environment modulations. These are all encoded in the sequences. The environment factors act as the filter to select certain sequential information out. For the EAK16-family peptides, the *p*H condition selects different kinds of patterns of charges. In this sense, the sequential pattern would be the most important factor to determine the structural switching. Some sequential signatures have also been observed in amyloid studies [47,48]. It is also possible to use the mutation or design to create novel certain sequences to fulfill certain expected structural switch for biology and nanomaterial applications. The phase diagram and stability analysis may act as useful theoretical methods to evaluate the validity of such kinds of systems.

IV. CONCLUSION

With a model including the backbone hydrogen bonds and electrostatic interactions, the thermodynamics of EAK16-family peptides are systematically studied with discrete molecular dynamics. The phase diagrams of these peptides related to the temperature and the strength of electrostatic interactions are evaluated. The different responses of peptides in their monomeric structures are presented. These results successfully explain the different aggregation behaviors of peptides. In more details, the contribution of the electrostatic interaction in peptide structure selection is calculated. The interplay between sequence-dependent electrostatic interaction and the backbone interaction determines the secondary structures of EAK16-family peptides in various kinds of conditions. The result outlines that the selection of various secondary structures for EAK16-family peptides is tightly related to the charge patterns of peptides. These peptides give some suggestive examples about how to stabilize or destabilize helical and hairpin structures. The information and method would be helpful for further analysis and designs of the sequence which may switch between various secondary structures.

ACKNOWLEDGMENTS

This work was supported by the National Basic Research Program of China (Grants No. 2006CB910302 and 2007CB814806), National Natural Science Foundation of China (Grants No. 10774069 and No. 10834002), and Natural Science Foundation of Jiangsu Province of China (Grant No. BK2009008). We thank Shanghai Supercomputer Center and High Performance Computing Center of Nanjing University for the computational supports. J.W. also thanks the support of FANEDD from MOE of China.

[1] K. Adermann, H. John, L. Standker, and W. G. Forssmann, Curr. Opin. Biotechnol. **15**, 599 (2004).
[2] H. Xiong, B. L. Buckwalter, H. M. Shich, and M. H. Hecht, Proc. Natl. Acad. Sci. U.S.A. **92**, 6349 (1995).
[3] P. P. Mager, B. Penke, R. Walter, T. Harkany, and W. Hartig, Curr. Med. Chem. **9**, 1763 (2002).
[4] A. L. Lau, A. Y. Yam, M. M. D. Michelitsch, X. Wang, C. Gao, R. J. Goodson, R. Shimizu, G. Timoteo, J. Hall, A. Medina-Selby, D. Coit, C. McCoin, B. Phelps, P. Wu, C. Hu, D. Chien, and D. Peretz, Proc. Natl. Acad. Sci. U.S.A. **104**, 11551 (2007).
[5] X. Zhao and S. Zhang, Trends Biotechnol. **22**, 470 (2004).
[6] X. Zhao and S. Zhang, Chem. Soc. Rev. **35**, 1105 (2006).
[7] M. Reches and E. Gazit, Nat. Nanotechnol. **1**, 195 (2006).
[8] R. V. Ulijn and A. M. Smith, Chem. Soc. Rev. **37**, 664 (2008).
[9] L. X. Zhong and W. C. Johnson, Jr., Proc. Natl. Acad. Sci. U.S.A. **89**, 4462 (1992).
[10] D. V. Waterhous and W. C. Johnson, Jr., Biochemistry **33**, 2121 (1994).
[11] L. M. Carrick, A. Aggeli, N. Boden, J. Fisher, E. Ingham, and T. A. Waigh, Tetrahedron **63**, 7457 (2007).
[12] S. Zhang, T. Holmes, C. Lockshin, and A. Rich, Proc. Natl. Acad. Sci. U.S.A. **90**, 3334 (1993).
[13] Y. Hong, R. L. Legge, S. Zhang, and P. Chen, Biomacromolecules **4**, 1433 (2003).
[14] S. Y. Fung, C. Keyes, J. Duhamel, and P. Chen, Biophys. J. **85**, 537 (2003).
[15] S. Jun, Y. Hong, H. Imamura, B. Y. Ha, J. Bechhoefer, and P. Chen, Biophys. J. **87**, 1249 (2004).
[16] Y. Hong, L. S. Lau, R. L. Legge, and P. Chen, J. Adhes. **80**, 913 (2004).
[17] Y. Hong, M. D. Pritzker, R. L. Legge, and P. Chen, Colloids Surf., B **46**, 152 (2005).
[18] H. Yang, M. Pritzker, S. Y. Fung, Y. Sheng, W. Wang, and P. Chen, Langmuir **22**, 8553 (2006).
[19] H. Yang, S. Fung, M. Pritzker, and P. Chen, J. Am. Chem. Soc. **129**, 12200 (2007).
[20] D. W. Zou, Z. X. Tie, C. M. Lu, M. Qin, X. M. Lu, M. Wang, W. Wang, and P. Chen, Biopolymers **93**, 318 (2010).
[21] Z. Q. Yan, J. Wang, and W. Wang, Proteins: Struct., Funct.,

Bioinf. **72**, 150 (2008).
[22] T. Kameda and S. Takada, Proc. Natl. Acad. Sci. U.S.A. **103**, 17765 (2006).
[23] K. Chockalingam, M. Blenner, and S. Banta, Protein Eng. Des. Sel. **20**, 155 (2007).
[24] S. Tsonchev, K. L. Niece, G. C. Schatz, M. A. Ratner, and S. I. Stupp, J. Phys. Chem. B **112**, 441 (2008).
[25] C. Keyes-Baig, J. Duhamel, S. Fung, J. Bezaire, and P. Chen, J. Am. Chem. Soc. **126**, 7522 (2004).
[26] H. Yang, S. Fung, M. Pritzker, and P. Chen, PLoS ONE **2**, e1325 (2007).
[27] H. Yang, S. Fung, W. Sun, S. Mikkelsen, M. Pritzker, and P. Chen, Biotechnol. Prog. **24**, 964 (2008).
[28] S. Dublin, Y. Zimenkov, and V. P. Conticello, Biochem. Soc. Trans. **37**, 653 (2009).
[29] P. Hamm, J. Helbing, and J. Bredenbeck, Annu. Rev. Phys. Chem. **59**, 291 (2008).
[30] S. Takada, Z. Luthey-Schulten, and P. G. Wolynes, J. Chem. Phys. **110**, 11616 (1999).
[31] A. Voegler Smith and C. K. Hall, Proteins **44**, 344 (2001).
[32] F. Ding, J. M. Borreguero, S. V. Buldyrey, H. E. Stanley, and N. V. Dokholyan, Proteins **53**, 220 (2003).
[33] F. Ding, S. V. Buldyrev, and N. V. Dokholyan, Biophys. J. **88**, 147 (2005).
[34] M. P. Allen and D. J. Tildesley, *Computer Simulation of Liquids* (Oxford University Press, Oxford, 1989).
[35] H. S. Chan and K. A. Dill, Proteins **30**, 2 (1998).
[36] P. Gilli, V. Bertolasi, V. Ferretti, and G. Gilli, J. Am. Chem. Soc. **122**, 10405 (2000).
[37] C. S. Wang, Y. Zhang, K. Gao, and Z. Z. Yang, J. Chem. Phys. **123**, 024307 (2005).
[38] M. M. Deshmukh and S. R. Gadre, J. Phys. Chem. A **113**, 7927 (2009).
[39] A. V. Finkelstein and O. B. Ptitsyn, *Protein Physics: A Course of Lectures* (Academic Press, New York, 2002).
[40] B. J. Alder and T. E. Wainwright, J. Chem. Phys. **31**, 459 (1959).
[41] D. C. Rapaport, J. Chem. Phys. **71**, 3299 (1979).
[42] Y. Q. Zhou and M. Karplus, Proc. Natl. Acad. Sci. U.S.A. **94**, 14429 (1997).
[43] S. W. Smith, C. K. Hall, and B. D. Freeman, J. Comput. Phys. **134**, 16 (1997).
[44] H. C. Andersen, J. Chem. Phys. **72**, 2384 (1980).
[45] Y. Q. Zhou and M. Karplus, J. Chem. Phys. **107**, 10691 (1997).
[46] A. M. Ferrenberg and R. H. Swendsen, Phys. Rev. Lett. **63**, 1195 (1989).
[47] B. M. Broome and M. H. Hecht, J. Mol. Biol. **296**, 961 (2000).
[48] A. Ghozlane, A. P. Joseph, A. Bornot, and A. G. De Brevern, Bioinformation **3**, 357 (2009).